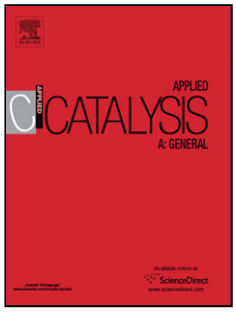

Title: Nanohybrid materials of titania nanosheets and plasmonic gold nanoparticles for effective hydrogen evolution

Author: Zheng Xing Xu Zong Teera Butburee Jian Pan Yang Bai Lianzhou Wang

PII: S0926-860X(16)30014-X
DOI: http://dx.doi.org/doi:10.1016/j.apcata.2016.01.014
Reference: APCATA 15729

To appear in: *Applied Catalysis A: General*

Received date: 30-8-2015
Revised date: 11-1-2016
Accepted date: 12-1-2016

Please cite this article as: Zheng Xing, Xu Zong, Teera Butburee, Jian Pan, Yang Bai, Lianzhou Wang, Nanohybrid materials of titania nanosheets and plasmonic gold nanoparticles for effective hydrogen evolution, Applied Catalysis A, General http://dx.doi.org/10.1016/j.apcata.2016.01.014

Nanohybrid materials of titania nanosheets and plasmonic gold nanoparticles for effective hydrogen evolution

Zheng Xing[a], Xu Zong[a], Teera Butburee[a], Jian Pan[b], Yang Bai[a], and Lianzhou Wang*[a]

[a] Nanomaterials Centre, School of Chemical Engineering and AIBN, The University of Queensland, Brisbane St Lucia, QLD 4072, Australia

[b] School of Chemical Engineering, Curtin University, Perth, Australia

*Corresponding author. Tel.: +61 7 336 54218; Fax: +61 7 336 54199; E-mail: l.wang@uq.edu.au

Graphical

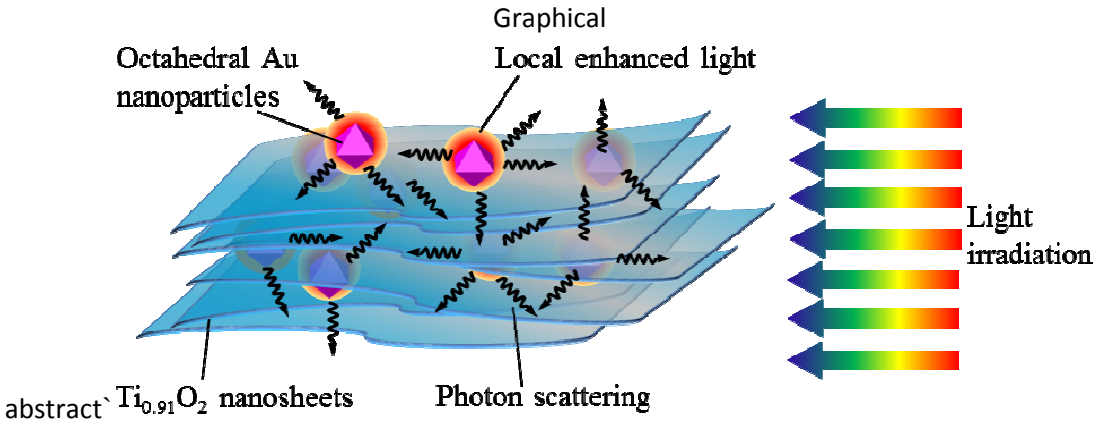

Abstract

A new type of nanocomposites containing titania and gold were prepared via the coupling between exfoliated $Ti_{0.91}O_2$ nanosheets and surfactant-capped Au nanoparticles, followed by flocculation and calcination. After hybridization with $Ti_{0.91}O_2$ nanosheets, octahedral Au nanoparticles were embedded

intimately into the matrix of titania, leading to a broad absorption peak assigned to surface plasmon resonance (SPR) effect in the visible region. The obtained nanocomposite exhibited remarkably improved photocatalytic hydrogen evolution performance compared to naked titania and conventional titania with photodeposited Au co-catalyst, due to the special SPR effect of the relatively large octahedral Au nanoparticles. Through control experiments, we demonstrated that the octahedral Au nanoparticles mainly functioned as local light intensifier and photon scattering agent.

Keywords

Nanocomposite, gold nanoparticles, titania nanosheets, surface plasmon resonance effect, photocatalysis, hydrogen

1. Introduction

Finding suitable semiconductors for solar fuel generation through the so-called artificial photosynthesis is the key to solving many environmental and energy-related issues. One of the most important and promising artificial photosynthesis processes is hydrogen production from solar water splitting, in which the clean hydrogen fuel can be generated from water.[1, 2] Among various semiconductor photocatalysts, TiO_2 has been the most intensively investigated one because of its low cost, photo- and chemical- stability, and high synthesis controllability.[3, 4] However, TiO_2 has a relatively wide band gap (ca. 3.2 eV) and thus can only absorb UV light while remains inactive in the visible region. To introduce visible light photocatalytic activities to TiO_2, guest species are often incorporated via two strategies: doping and heterostructuring. Doping is an effective way to incorporate guest atoms into the crystal lattice of TiO_2 and render visible light absorption. Nevertheless, doping often creates crystal defects, which may act as recombination centres for photoinduced electrons and holes.[5]

Unlike doping, heterostructuring allows the incorporation of relatively bulky guest species by directly combining different materials with proper energy band alignment. A good example is the metal/semiconductor heterogeneous structure, in which noble metals such as Pt[6] and Au[7, 8] are loaded onto semiconductors as cocatalyst, and such a structure can provide both effective charge separation and active sites for water splitting. In addition, noble metal nanoparticles (NPs) such as Ag, Au, Cu etc. have attracted much interest recently due to their unique surface plasmon resonance (SPR) properties.[4, 9, 10] SPR is defined as the collective oscillation of free electrons when the frequency of incident photons approaches the natural frequency of surface electron oscillation.[1] SPR effect can induce a very strong localized electric field near the noble metal nanostructures, and it can be significantly influenced by the size, shape and embedding medium.[11-15] Of those noble metals, Au

draws particular attention as it has strong SPR effect in visible region and many researchers have successfully synthesized Au NPs with varied sizes and diverse morphologies.[15-17]

With the arising interest in the SPR properties of Au, many semiconductor/Au composites have been investigated in terms of visible light activities and it was found that in many cases the enhancement of photocatalytic activities occurred at wavelengths corresponding to the metal SPR.[18-20] The enhancement induced by SPR has been contributed to three proposed mechanisms: direct charge injection from Au NPs to semiconductors, strong SPR-induced near-field electromagnetic energy and effective photon scattering.[11] In order to verify these mechanisms, titania-supported Au NPs have been prepared in various methods: direct adsorption of pre-synthesized Au colloids, photo-deposition, deposition-precipitation, core-shell structure construction, etc.[21] However, there are two great limitations of these methods. First, generally the size and morphologies of Au NPs cannot be precisely controlled owing to the absence of morphology-control reagents. In most cases, the Au NPs are of spherical shape. Second, Au NPs tend to aggregate or grow up at the surface of TiO_2 particles during the composite material synthesis, which will lead to the variation of SPR properties. This issue can be solved by separating gold nanoparticles with titania, and thus forming a structure in which Au nanoparticles are embedded into titania, for example, core-shell structures.[22-25]

Although constructing core-shell structure provides an effective way to separate Au NPs, the coating process of tiania shell often involves careful and complex chemical and physical control.[26] Hata et al. reported a general method to intercalate Au NPs into galleries of layered materials such as Dion-Jacobson layered perovskite $HCa_2Nb_3O_{10}$ via pre-intercalation of tetrabutylammonium hydroxide (TBAOH) and polyallylamine (PAA) to enlarge the interlayer space.[27] This general method promises a simpler method of embedding Au NPs into semiconductor matrix compared to the core-shell structure. Nevertheless, the size of gold is greatly restricted because the extent of gallery expansion is very limited. Here we report a facile way to prepare titania-gold nanocomposite materials with easily tuneable Au NPs. By thorough mixing of exfoliated titania ($Ti_{0.91}O_2$) nanosheets (NSs) and pre-synthesized Au NPs followed by flocculation and calcination, leading to the octahedral Au NPs embedded intimately in the matrix of anatase titania. The shapes and sizes of Au NPs can be simply controlled during the synthesis process, so special SPR properties can intentionally introduced into the composite material. To demonstrate this method, we successfully synthesized an Au/TiO_2 composite material containing relatively large octahedral Au NPs. The Au NPs were well separated in the nanocomposite. Moreover, the octahedral Au NPs provide good SPR-induced optical properties such as localized light intensity enhancement and photon scattering improvement, and thus the as-prepared nanocomposite exhibited dramatically improved hydrogen evolution performance compared to the naked titania.

2. Experimental

All chemicals were purchased from Sigma-Aldrich including cesium carbonate (99.9%), titanium (IV) dioxide (99%), hydrochloric acid (37%), tetrabutylammonium hydroxide solution (40% in water), cetyltrimethylammonium bromide (99%), gold (III) chloride hydrate (99.999%), trisodium citrate (99%), chloroplatinic acid hydrate (99.9%) and sodium borohydride (99%). They were used without further purification.

2.1 Preparation of nanobybrid

Titania nanosheets suspension ($Ti_{0.91}O_2$ NSs) was prepared according to previous reports by Sasaki's group.[28-31] In a typical synthesis process, the layered $Cs_{0.68}Ti_{1.83}O_4$ precursor was first obtained by solid state reaction, followed by proton-exchange to $H_{0.68}Ti_{1.83}O_4 \cdot H_2O$ in hydrochloric acid and a delamination step in the presence of tetrabutylammonium cations (TBA^+). Stoichiometric mixture of Cs_2CO_3 and TiO_2 were thoroughly ground before heated at 1033K for 30 mins. Then the sample was reground and reheated at 1033K for another 12 hours. The obtained $Cs_{0.68}Ti_{1.83}O_4$ titanate precursor was subsequently placed in excess amount of hydrochloric acid (1M) and stirred vigorously for three days. The hydrochloric acid was refreshed every 24 hours and the proton-exchanged titanate $H_{0.68}Ti_{1.83}O_4 \cdot H_2O$ can be collected by centrifugation and wash with deionised water. The dried $H_{0.68}Ti_{1.83}O_4 \cdot H_2O$ was re-dispersed in tetrabutylammonium hydroxide (TBAOH) solution containing same amount of TBA+ as protons, and the white suspension was shaked for over 7 days. To remove the un-delaminated precursors, the suspension was centrifuged under 4700 rpm and the supernatant suspension was collected for use. The concentration of $Ti_{0.91}O_2$ NSs suspension is ca. 1.79 g/L.

Octahedral Au nanoparticles (NPs) were synthesized via a simple hydrothermal method reported before.[32] In a typical synthesis procedure, 0.055 g of cetyltrimethylammonium bromide (CTAB) was first dissolved in 9.7 mL of deionised water, and then 250 μL of 0.01 M $HAuCl_4$ and 50 μL of 0.1 M trisodium citrate were added. The solution was then transferred to a Teflon-lined autoclave and heated at 383K in an oven for 48 hours. The concentration of Au NPs suspension is ca. 0.05 g/L. The Au NPs with tunable sizes and shapes can be prepared using the methods in the literature, which will affect the photocatalytic performance of the resultant composite photocatalysts. [33]

Under vigorous stirring, 2 mL of Au NPs suspension was added dropwise to 50 mL of $Ti_{0.91}O_2$ NSs suspension. After 30 mins of stirring to reach a uniform mixture of NPs and NSs, hydrochloric acid (1 M) were added to flocculate the NSs coupled with NPs. The nanohybrids were centrifuged, washed with deionised water and ethanol for several times and dried in a 100 °C oven. The as-prepared sample is denoted as O-Au-NS. Then O-Au-NS was placed in an alumina crucible and calcined at 723 K for 2 hours, which is denoted as O-Au-A. The ratio of Au in both O-Au-NS and O-Au-A is calculated to be around 0.11 wt%.

As comparison, two types of nanohybrids between $Ti_{0.91}O_2$ NSs and irregular Au NPs were prepared, in which the ratio of Au was kept to be 0.11 wt%. One sample was prepared by direct deposition of Au particles onto $Ti_{0.91}O_2$ NSs via photo-deposition, flocculation with protons and calcination. First, 2 mL of $HAuCl_4$ solution (0.01 M) and ethanol were added to 50 mL of $Ti_{0.91}O_2$ NSs suspension. Under stirring, the suspension was illuminated by Xenon lamp for 6 hours, and flocculated with hydrochloric acid (1 M). To ensure that $HAuCl_4$ has been completely reduced to Au, the supernatant solution after centrifugation was treated with $NaBH_4$ solution and its absorption spectrum was measured by a UV-Vis spectrometer. The flocculated product was then calcined at 723 K and this sample was denoted as Au-A-1.

The other sample was prepared by photo-depositing gold onto restacked NSs after calcination. 50 mL of $Ti_{0.91}O_2$ NSs suspension was first flocculated with hydrochloric acid (1 M), followed by calcination 723 K for 2 hours. The obtained product (A) was then dispersed in ethanol solution containing 2 mL of $HAuCl_4$ (0.01M), and illuminated by Xenon lamp for 6 hours. Similar method was implemented to ensure the complete reduction of $HAuCl_4$ as used in the preparation of Au-A-1. This sample was denoted as Au-A-2. **Scheme 1** shows the synthesis procedures of all samples.

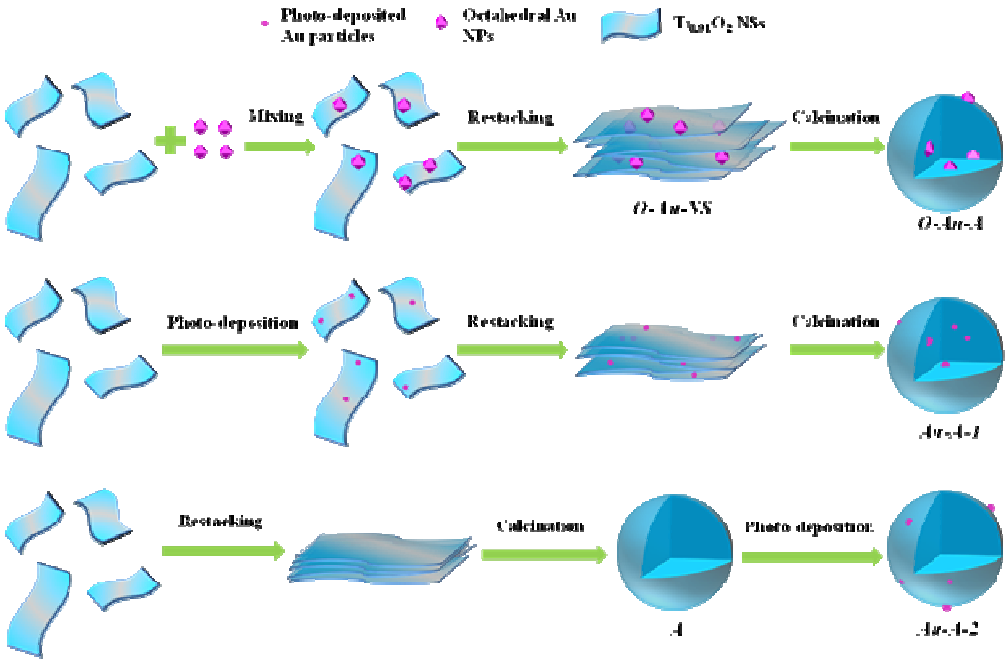

Scheme 1. Schematics of the synthesis routes of different hybrid samples.

2.2 Characterizations

The crystalline structure of samples was characterized by powder X-ray diffraction (XRD, Rigaku Miniflex) with Co Kα (λ= 1.78897 Å) radiation. The morphology of different samples was examined by transmission electron microscopy (TEM, JEOL 1010 at 100 kV) and scanning electron microscopy (SEM, JEOL JSM-7001F at 20 kV). The light absorption of samples was characterized by UV-Vis

spectrometer (Shimadzu 2200). X-ray photoelectron spectroscopy (XPS, Thermo Escalab 250, a monochromatic Al KR x-ray source) was carried out to determine the chemical composition of the as-prepared nanohybrid materials and the chemical status of various species. The Brunauer-Emmett-Teller (BET) surface area was measured using nitrogen adsorption apparatus (Tristar 3030, Micromeritics Instrument Corporation). The sizes and surface charges of sample particles were measured using a zetasizer (Zetasizer Nano ZS, Malvern Instruments).

2.3 Photocatalytic activity measurement

The photocatalytic reactions were carried out in a quartz reaction cell connected to a closed gas circulation and evacuation system. 40mg of catalyst was suspended in 300 ml aqueous solution containing 60 ml of ethanol, and H_2PtCl_6 solution containing 1wt% of Pt was added to the suspension. Before the reaction starts, the whole system was thoroughly degassed. The quartz reactor was irradiated by a 300 W Xe lamp (Beijing Trusttech Co. Ltd., PLS-SXE-300UV) from its top. The light spectrum produced by the Xe lamp is shown as Figure S1. A water filter was applied to the top of the reactor in order to remove infrared light. The temperature of the reactor was maintained at 293±5 K by a cooling water cycle system. The evolved hydrogen gas was collected by a sampling device and tested by gas chromatography (GC) with Ar as the carrier gas.

3. Results and discussion

3.1 Formation and microstructure of the nanohybrid materials

The $Ti_{0.91}O_2$ NSs used in this work were obtained from exfoliation of a lepidocrocite-type layered protonic titanate, $H_{0.68}Ti_{1.83}O_4 \cdot H_2O$ in aqueous solution of TBAOH.[28, 29] The as-prepared NSs possess a thickness of 0.75 nm taking the outer edge of surface oxygen atoms, and negative charges of ca. -39 mV.[31, 34] TEM image in Figure 1a confirmed the ultrathin nature of $Ti_{0.91}O_2$ NSs and their extremely high two-dimensional anisotropy.

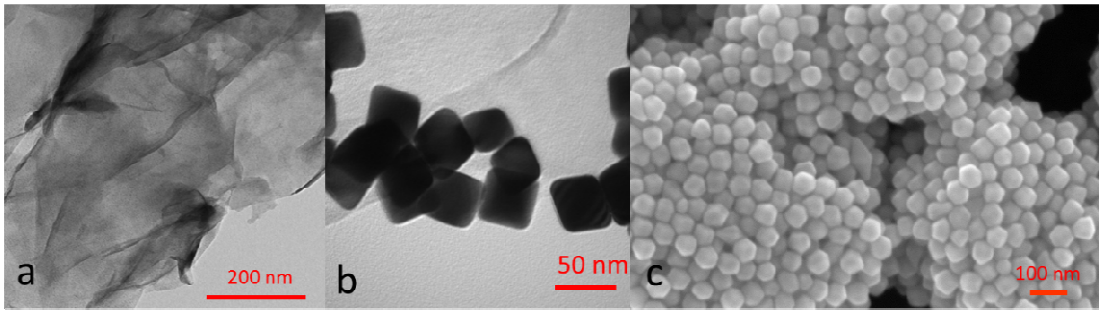

Figure 1. (a) TEM image of exfoliated $Ti_{0.91}O_2$ NSs. (b) TEM image and (c) SEM image of octahedral Au NPs prepared via hydrothermal method.

The pre-synthesized Au NPs possessed octahedral morphology and relatively uniform size of ca. 70 nm, as confirm by the TEM and SEM images (Figure 1b-c). To further confirm the size of the

octahedral Au NPs, dynamic light scattering (DLS) technique was implemented. The octahedral Au NPs have very uniform size distribution around 69 nm, which corresponded well to the observations in TEM. Due to the presence of ammonium group in the capping agent, that is, cetyltrimethylammonium bromide (CTAB), the Au NPs will carry positive charges. Zeta potential measurement showed that the octahedral Au NPs carried a positive charge of +59 mV.

The synthesis routes and denotation of all the samples are shown in Scheme 1. When the octahedral Au NPs were added to NSs suspension, Au NPs were attracted to the surface of NSs as a result of electrostatic force. Upon the addition of hydrochloric acid, the NSs attached with octahedral Au NPs flocculated and settled, leaving the supernatant solution colourless. The flocculated NSs remained pink-ish after drying at 100 °C (O-Au-NS) and calcination at 450 °C (O-Au-A). As a comparison, two other types of Au-TiO_2 composites were also prepared, in which Au NPs were introduced to different locations in the composites via direct photo-deposition. In one composite, Au particles were directly photo-deposited onto NSs before calcination, so most of the Au particles were distributed in the interior of the final composite (Au-A-1). In the other composite, however, flocculated NSs were first calcined to anatase particles (A) before being photo-deposited with Au particles (Au-A-2), so the Au particles will be dispersed only on the surface of Au-A-2. It should be noticed that all nanocomposites contain the same amount of Au (0.11 wt%).

Figure 2 illustrates the XRD patterns for all synthesized nanocomposites. The XRD pattern of O-Au-NS exhibited a (010) peak at 2θ=8.74 °, corresponding to d spacing of 1.17 nm (Figure 2a). There were no distinct peaks assigned to titania phase in O-Au-NS, which reflects the lack of three-dimensional order in long distance. Its XRD pattern is typical for intercalated complex with lattice expansion along the b-axis.[35, 36] The relatively broader peaks of the nanocomposite resulted from elastic deformation of host layers upon lattice expansion.[37] The XRD result demonstrated the randomly restacked structure of NSs in O-Au-NS. After calcination at 450°C, the (010) peak disappeared while peaks assigned to anatase phase evolved in the XRD pattern of O-Au-A (Figure 2b), which indicates that the stacked sheets structure collapsed to form an anatase crystal structure. It has been previously demonstrated by Fukuda et al. that a very thin film made of several layers of monolayered titania NSs could transform into anatase phase at elevated temperatures and the transformation temperature decreased for thicker films.[38] The films composed of more than five layers of NSs were found to transform to anatase at 400-500 °C. Considering that our nanocomposite was prepared by stacking multilayers of $Ti_{0.91}O_2$ NSs, calcination at 450°C could induce the recrystallization of titania NSs to form three-dimensional crystalline anatase structure. It is noted that no peaks of Au appeared in the XRD pattern of either O-Au-NS or O-Au-A, which we believe is due to the fact that most Au NPs were sandwiched between $Ti_{0.91}O_2$ NSs. Similar to O-Au-A, both Au-A-1 and Au-A-2 showed peaks of anatase phase in their XRD patterns, but a small peak at 2Θ=52 ° assigned to Au appeared (Figure 2c and 2d).

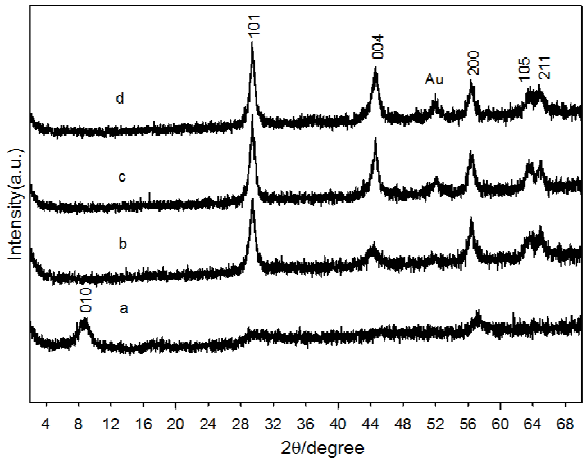

Figure 2. XRD patterns of (a) O-Au-NS, (b) O-Au-A, (c) Au-A-1, and (d) Au-A-2.

To investigate the morphology of the nanocomposites, TEM was performed. In O-Au-NS, the ultrathin NSs formed a randomly stacked structure, in which the Au NPs were extremely difficult to find (Figure 3a and 3b). This is in good agreement with our observation in the XRD pattern. After very careful searching in TEM, we only found very few octahedral Au NPs wrapped by NSs, and all NPs were well separated because of their scarcity and thorough mixing with NSs. After calcination, the stacking structure of NSs collapsed due to recrystallization, transforming to irregular-shaped porous anatase particles in O-Au-A (Figure 3c). Similar to O-Au-NS, Au NPs were very scarce and we were only able find to one after very long time of searching in TEM (Figure 3d). We believe that most Au NPs were embedded into the matrix of anatase after calcination as indicated in the XRD pattern. It is noted that after calcination, the morphology and size of Au NPs remained unchanged. We assign the stability of Au NPs to the protection of titania surrounding Au NPs. TEM images of Au-A-1 and Au-A-2 are presented in Figure 3e and 3f, respectively, and it can be seen that the photo-deposited Au particles were of irregular spherical shape and possessed smaller sizes compared to the octahedral Au NPs.

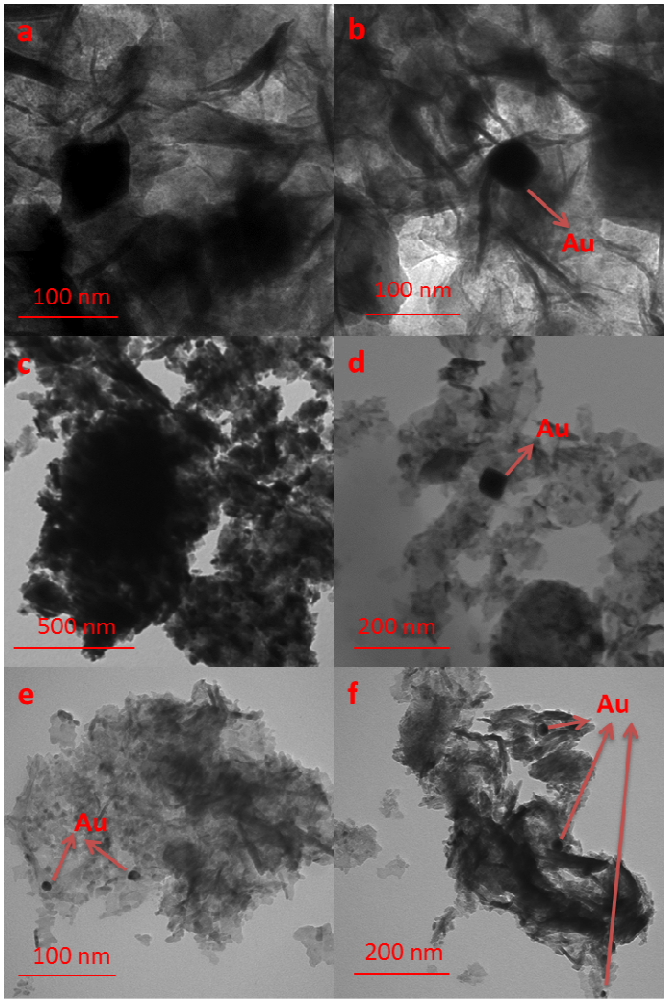

Figure 3. TEM images of (a) and (b) O-Au-NS, (c) and (d) O-Au-A, (e) Au-A-1 and (f) Au-A-2.

Nitrogen adsorption-desorption isotherm measurements were carried out to further study the microstructure of the nanocomposites. As shown in Figure 4, all nanocomposites exhibited Type IV isotherms, corresponding to mesoporous structure.[39] Isotherm of O-Au-NS showed a H3-type hysteresis loop in the IUPAC classification,[38] revealing the presence of slit-shaped pores. Such type of isotherms was observed in nickel oxide pillared titania NSs before, which highlighted the existence of open slit-shaped capillaries with very wide bodies and narrow short necks.[37] In addition, the hysteresis loops of O-Au-NS appeared in the relative pressure region of $p/p_0>0.5$, which suggests that the majority of the porosity originated from mesopores in the randomly restacked structure.[35, 40] After calcination, an H1-type hysteresis loop appeared in the isotherms of all nanocomposites containing anatase phase (O-Au-A, Au-A-1 and Au-A-2), indicating that their microstructure changed to agglomerates of spheres.[39] All results from nitrogen adsorption-desorption isotherms agreed well with our previous analysis of XRD and TEM data. Table 1 summarizes the surface area of all nanohybrids according to BET equation based fitting analysis. Calcination caused collapse of the stacking structure and agglomeration of anatase particles, which is reflected in the drop in surface area of O-Au-A (84.4 m^2/g) compared to O-Au-NS (135.4 m^2/g).

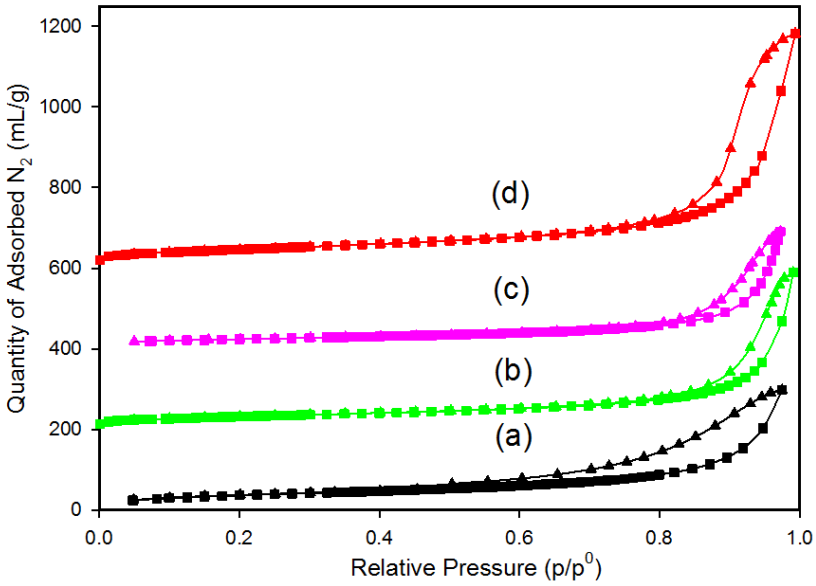

Figure 4. Nitrogen adsorption-desorption isotherms of the nanocomposites: (a) O-Au-NS, (b) Au-A-2, (c) O-Au-A, and (d) Au-A-1.

Table 1. BET surface areas of the composite materials.

Sample	BET surface area (m^2/g)
O-Au-NS	135.4
O-Au-A	84.4
Au-A-1	166.1
Au-A-2	114.0

3.2 Chemical state analysis

To investigate the chemical states of Au present in the nanohybrids, the Au 4f levels were measured using XPS. As shown in Figure 5, the peaks of Au $4f_{7/2}$ located at 83.3-83.4 eV are close to metallic Au^0 $4f_{7/2}$ (84.0 eV), and different from Au^+ $4f_{7/2}$ (85.2 eV) and Au^{3+} $4f_{7/2}$ (86.7 eV),[41, 42] which confirms the metallic state of Au. The surface Au:Ti atomic ratios detected by XPS in Au-A-2 and Au-A-1 are 0.018:1 and 0.0033:1 respectively, which verified the fact that more Au particles existed at the surface of Au-A-2 compared to Au-A-1. However, no signals of Au 4f were detected in XPS spectra of O-Au-NS and O-Au-A. The most possible reason is that the majority of Au NPs were wrapped, so the signals of Au NPs were screened by titania. We implemented Ar ion-sputtering to remove the top surface layers of O-Au-NS and O-Au-A, but the signals of Au were still not detected even though a 40 nm-thick surface layer was removed. Considering the scarcity of Au NPs and the small detection area of XPS technique, this phenomenon is understandable.

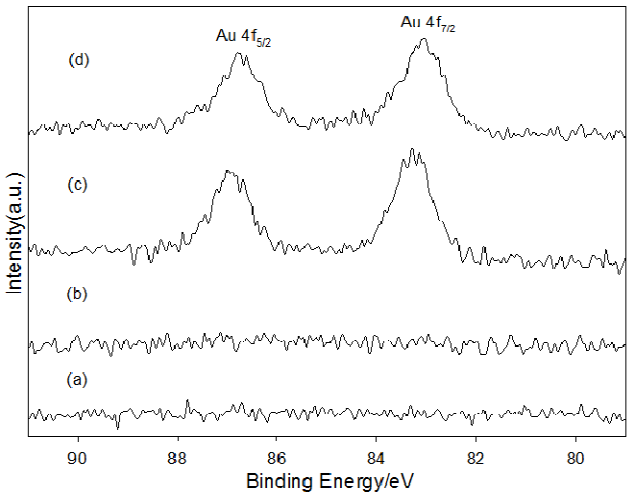

Figure 5. High resolution XPS spectra of Au 4f in (a) O-Au-NS, (b) O-Au-A, (c) Au-A-2 and (d) Au-A-1.

3.3 Light absorption properties analysis

Figure 6 shows the overall light absorption spectra for all composites and naked titania (A). All composites containing Au particles exhibit a broad absorption peak in the wavelength range of 500-600 nm, which can be assigned to the SPR effect of Au particles. A has an absorption edge at a wavelength of 418 nm corresponding to a band gap of 2.97 eV (Figure 6a), which is slightly smaller than general band gap measured of anatase (ca. 3.2 eV). Since A was prepared by calcining flocculated NSs and some organic chemicals like TBA^+ might be incorporated into flocculated NSs, small amount of C may exist in A, leading to the extended light absorption above 400 nm. All the other composites possess larger band gaps of around 3.12-3.26 eV, compared to A, which is probably owing to the interaction between Au and titania.[43-45] O-Au-NS (Figure 6c) and O-Au-A (Figure 6b) exhibited slightly red-shifted SPR peaks at around 565 nm compared to those of Au-A-1 (Figure 6e) and Au-A-2 (Figure 6d) at around 550 nm, which is due to the presence of larger octahedral Au NPs in the former two nanocomposites. SPR peak was reported to shift towards longer wavelength with the increasing size of Au NPs,[15, 18, 46, 47] and so the SPR peak shift agreed well with the observations from TEM. Moreover, Noguez reported that compared to polyhedral nanoparticles, spherical ones will have blue-shifted SPR peaks.[48] There was no obvious change of the SPR peak position after O-Au-NS was calcined, which again reflects the retainment of the size and shape of octahedral Au NPs.

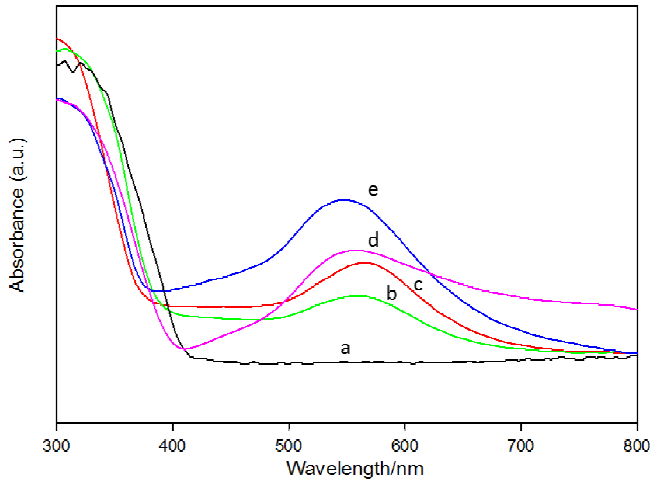

Figure 6. UV-Vis absorption spectra of the composites: (a) A, (b) O-Au-A, (c) O-Au-NS, (d) AU-A-2 and (e) Au-A-1.

3.4 Photocatalytic hydrogen production test

The average hydrogen evolution rates for all samples are shown in Figure 7. The Xe lamp produces both UV light and visible light (Figure S2). Naked titania A can only produce H_2 at a low rate of 1474 $\mu mol \cdot h^{-1} \cdot g^{-1}$. O-Au-NS showed very low activities, which is mainly because of its low crystallinity. However, after calcination, the hydrogen evolution rate dramatically increased (up to over 270 times), to 6753 $\mu mol \cdot h^{-1} \cdot g^{-1}$, which is 3.6 times faster than A. O-Au-A can also produce hydrogen faster than Au-A-1 (5071 $\mu mol \cdot h^{-1} \cdot g^{-1}$) and Au-A-2 (3443 $\mu mol \cdot h^{-1} \cdot g^{-1}$).

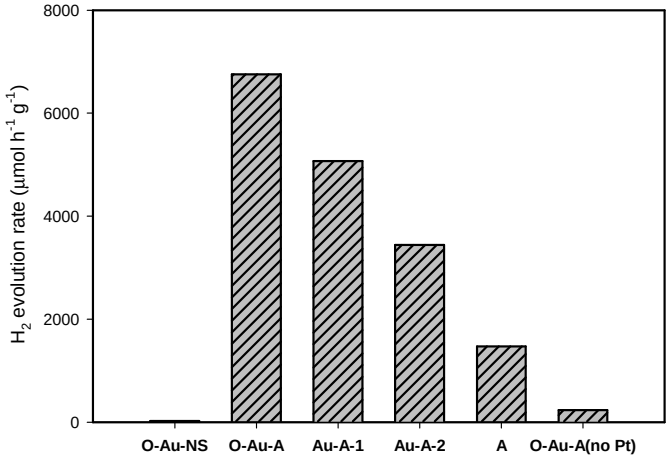

Figure 7. Normalized average hydrogen evolution rates for all samples prepared. Experimental conditions: 40 mg of catalyst powder photo-deposited with 1wt% Pt (except the last one) was dispersed in 300 mL of aqueous ethanol solution (20 vol%), light source was 300 W Xenon lamp.

3.5 Analysis on the role of Au NPs

The most efficient nanocomposite, O-Au-A, can evolve hydrogen more than 3.6 times faster than naked titania A, even though the ratio of Au is extremely low (ca. 0.11 wt%). The phenomenon indicates the vital role of octahedral Au NPs in the photocatalytic reaction. As mentioned earlier,

several mechanisms regarding the role of Au NPs have been proposed by researchers. We conducted some experiments to investigate the roles of Au NPs in our material system.

Conventionally, Au in a metal-semiconductor composite system can act as a sink for photoinduced electrons and catalyses the reduction of protons, in which way Au improves the photocatalytic performance as a co-catalyst. However, in order to effectively act as co-catalyst, Au must exist in the interfacial region between semiconductors and the electrolyte. In a control experiment, we conducted hydrogen evolution with O-Au-A in the absence of Pt. Surprisingly, O-Au-A alone produced even less hydrogen compared to A deposited with Pt, as shown in Figure 7. This phenomenon can be explained in the way that due to the scarcity of Au NPs at the surface of O-Au-A, the ability of octahedral Au NPs as co-catalyst is very limited in the nanocomposite. However, octahedral Au NPs may still partly act as co-catalyst, which is a minor function of Au NPs in our nanocomposite system.

In the direct electron injection mechanism, Au NPs undergo SPR-induced excitation upon visible light irradiation and electrons in the surface plasmon (SP) states possess enough energy to be injected to the conduction band of semiconductors. This mechanism has been very controversial in Au-TiO_2 composite systems. Even though water splitting under visible light has been reported by several groups,[2, 4, 10] no direct evidence of electron transfer between Au particles and titania were provided. At the same time, the possibility of photoexcitation of Au NPs by visible light has been ruled out in several papers of Cronin's Group in recent years.[41, 49, 50] They claimed that there is no highest occupied molecular orbital-lowest unoccupied molecular orbital (HOMO-LUMO) energy band configuration like semiconductors in a plasmon excitation, so the visible activities originated from the sub-bandgap transition in TiO_2 with some dopants. In another control experiment, we equipped the Xe lamp with a 420 nm cut-off filter so only visible light can reach the reactor. For all samples, no hydrogen can be detected. Since titania cannot be excited by photons with wavelength longer than 420 nm, Au NPs did not seem to act as visible light sensitizer in our case.[51]

From the discussion above, octahedral Au NPs seem to work insignificantly as co-catalyst and hardly as visible photosensitizer. However, the dramatically improved hydrogen production capability of O-Au-A compared to A highlights the importance of octahedral Au NPs. Therefore, in our opinion, the other two effects of SPR, that is, intensified localized electric field and photon scattering, are likely to work at the same time to enhance the photocatalytic water splitting. The mechanism of the two effects is shown in Scheme 2. Upon SPR-induced excitation of Au NPs, charges are concentrated at the metal-semiconductor interface, yielding a dramatic amplification of localized electric field.[13] In this case, Au NPs essentially act as light concentrators and the localized field is distributed very unevenly, with the highest intensity at the surface of Au NPs and decreasing exponentially within 20-30 nm from the surface and linearly further away.[11] Through finite-difference time-domain (FDTD) simulation, Christopher et al. reported that an isolated Ag nanocube with an edge length of 75 nm can

produce a SPR-induced electric fields with intensity of ~10^3 times larger than the incident photon flux while two same nanocubes with 1 nm distance can enhance the light intensity up to ~10^6 times.[51] Using similar FDTD simulation, Liu et al. also found that the localized SPR-induced electric field intensity in their Au-anodic TiO_2 film can reach up to 1000 times that of the incident electric field intensity.[49] This largely enhanced local light intensity will promote photoexcitation of semiconductor and thus produce more electrons and holes, considering that the charger pair formation rate is proportional to the local light intensity.[11] In addition, plasmonic nanostructure acts a nanomirror in the composites, which can scatter the resonant photons to have longer lifetime in the system.[11, 53, 54] In this way, photons are given many more passes through the materials and can be utilized more efficiently. As shown in Figure 8, O-Au-A showed significantly better light scattering behaviour compared to those of samples Au-A-1 and Au-A-2,[55] which can be elucidated by the fact that the photon scattering effect become more significant with the increase of the size of Au NPs.[54] This drastic photon scattering effect can explain why O-Au-A showed better photocatalytic performance than Au-A-1 and Au-A-2, that is, the larger octahedral Au NPs embedded in O-Au-A can scatter more photons throughout the catalyst particles efficiently than the small irregular-spherical Au particles in Au-A-1 and Au-A-2, which subsequently result in more efficient utilization of the light for initiating photocatalytic activity. Based on the above discussion, it is interesting to predict the effect of Au size on the photocatalytic activity of the composites. Further increase of the size of the Au NPs within a range will increase the photocatalytic activity due to enhanced photon scattering. However, overly large Au NPs can lead to weakened SPR effect, and the mismatch between SPR spectrum and TiO_2 absorption spectrum may result in deteriorated photocatalytic performance. [54]

So to briefly conclude, we believe that Au NPs mainly function to enhance local light intensity and scatter photons in our system. On the contrary, the possibility of photosensitization of Au NPs can be ruled out and the role as co-catalyst is minor.

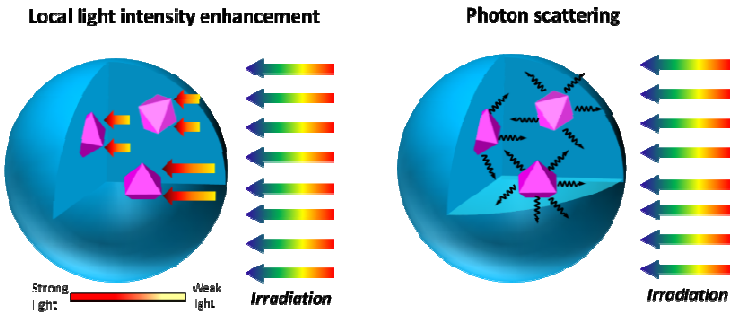

Scheme 2. Schematics of the two effects of octahedral Au NPs: Local light intensity enhancement and photon scattering. (Blue spheres: titania matrix, pink octahedral particles: Au nanoparticles)

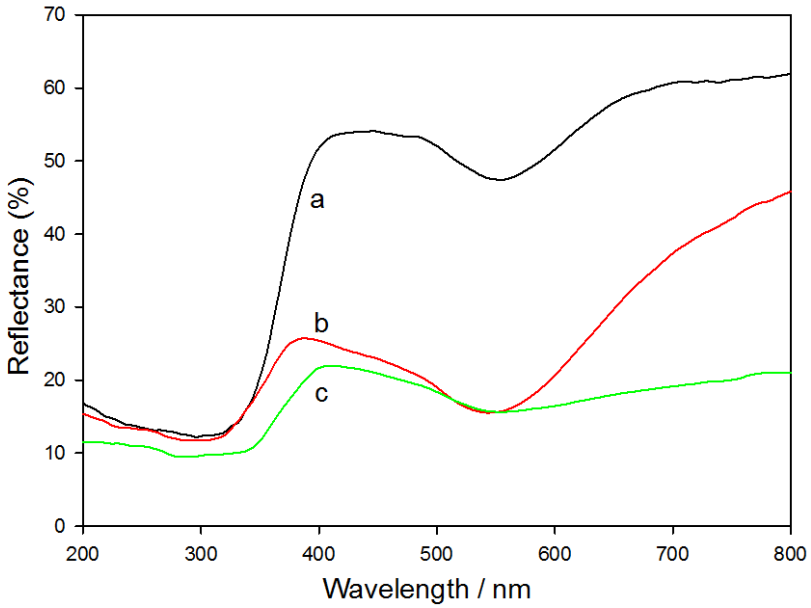

Figure 8. UV-Visible reflectance spectra of (a) O-Au-A, (b) Au-A-1 and (c) Au-A-2.

4. Conclusions

A new type of Au-TiO_2 nanocomposites with well dispersed octahedral Au NPs of relatively large particle size were developed. By using exfoliated $Ti_{0.91}O_2$ NSs and pre-synthesized Au NPs as the starting materials, it is easy to achieve nanocomposite with intimately mixed Au NPs with matrix of anatase titania. The synthesized nanocomposite showed much better photocatalytic hydrogen evolution performance compared to naked titania and titania photo-deposited with Au due to the excellent SPR properties of the pre-synthesized octahedral Au NPs. This strategy provides some important information for the development of nanocomposite photocatalysts, which can be applicable to both other nanosheets ($Nb_6O_{17}^{4-}$, $Ca_2Nb_3O_{10}^{-}$, etc.) and other plasmonic metal NPs (Ag, Cu, etc.).

Acknowledgements

This project was supported by Australian Research Council (through its DP and Future Fellowship programs).

Reference

[1] H. Wang, T.T. You, W.W. Shi, J.H. Li, L. Guo, Au/TiO_2/Au as a Plasmonic Coupling Photocatalyst, J. Phys. Chem. C, 116 (2012) 6490-6494.

[2] S. Mubeen, J. Lee, N. Singh, S. Krämer, G.D. Stucky, M. Moskovits, An autonomous photosynthetic device in which all charge carriers derive from surface plasmons, Nat. Nanotech., 8 (2013) 247-251.

[3] G. Liu, L. Wang, H.G. Yang, H.M. Cheng, G.Q.M. Lu, Titania-based photocatalysts-crystal growth, doping and heterostructuring, J. Mater. Chem., 20 (2009) 831-843.

[4] C.u. Gomes Silva, R. Juárez, T. Marino, R. Molinari, H. García, Influence of excitation wavelength (UV or visible light) on the photocatalytic activity of titania containing gold nanoparticles for the generation of hydrogen or oxygen from water, J. Am. Chem. Soc., 133 (2010) 595-602.

[5] H. Irie, Y. Watanabe, K. Hashimoto, Nitrogen-concentration dependence on photocatalytic activity of $TiO_{2-x}N_x$ powders, J. Phys. Chem. B, 107 (2003) 5483-5486.

[6] X.W. Wang, G. Liu, Z.G. Chen, F. Li, L.Z. Wang, G.Q. Lu, H.M. Cheng, Enhanced photocatalytic hydrogen evolution by prolonging the lifetime of carriers in ZnO/CdS heterostructures, Chem. Commun., (2009) 3452-3454.

[7] G.R. Bamwenda, S. Tsubota, T. Nakamura, M. Haruta, Photoassisted hydrogen production from a water-ethanol solution: a comparison of activities of Au-TiO_2 and Pt-TiO_2, J. Photochem. Photobiol. A, 89 (1995) 177-189.

[8] T. Puangpetch, S. Chavadej, T. Sreethawong, Hydrogen production over Au-loaded mesoporous-assembled $SrTiO_3$ nanocrystal photocatalyst: Effects of molecular structure and chemical properties of hole scavengers, Energy Conv. Manag., 52 (2011) 2256-2261.

[9] M. Murdoch, G. Waterhouse, M. Nadeem, J. Metson, M. Keane, R. Howe, J. Llorca, H. Idriss, The effect of gold loading and particle size on photocatalytic hydrogen production from ethanol over Au/TiO_2 nanoparticles, Nat. Chem., 3 (2011) 489-492.

[10] H. Yuzawa, T. Yoshida, H. Yoshida, Gold nanoparticles on titanium oxide effective for photocatalytic hydrogen formation under visible light, Appl. Catal. B, 115–116 (2012) 294-302.

[11] S. Linic, P. Christopher, D.B. Ingram, Plasmonic-metal nanostructures for efficient conversion of solar to chemical energy, Nat. Mater., 10 (2011) 911-921.

[12] K.L. Kelly, E. Coronado, L.L. Zhao, G.C. Schatz, The optical properties of metal nanoparticles: the influence of size, shape, and dielectric environment, J. Phys. Chem. B, 107 (2003) 668-677.

[13] Y. Xia, N.J. Halas, Shape-controlled synthesis and surface plasmonic properties of metallic nanostructures, MRS Bull., 30 (2005) 338-348.

[14] N. Halas, Playing with plasmons: tuning the optical resonant properties of metallic nanoshells, MRS Bull., 30 (2005) 362-367.

[15] C.J. Orendorff, T.K. Sau, C.J. Murphy, Shape-dependent plasmon-resonant gold nanoparticles, Small, 2 (2006) 636-639.

[16] P.J. Chung, L.M. Lyu, M.H. Huang, Seed-Mediated and Iodide-Assisted Synthesis of Gold Nanocrystals with Systematic Shape Evolution from Rhombic Dodecahedral to Octahedral Structures, Chem.-Eur. J., 17 (2011) 9746-9752.

[17] M.L. Personick, M.R. Langille, J. Zhang, C.A. Mirkin, Shape Control of Gold Nanoparticles by Silver Underpotential Deposition, Nano Lett., 11 (2011) 3394-3398.

[18] E. Kowalska, O.O.P. Mahaney, R. Abe, B. Ohtani, Visible-light-induced photocatalysis through surface plasmon excitation of gold on titania surfaces, Phys. Chem. Chem. Phys., 12 (2010) 2344-2355.

[19] N. Sakai, Y. Fujiwara, Y. Takahashi, T. Tatsuma, Plasmon-Resonance-Based Generation of Cathodic Photocurrent at Electrodeposited Gold Nanoparticles Coated with TiO_2 Films, ChemPhysChem, 10 (2009) 766-769.

[20] Y. Tian, T. Tatsuma, Mechanisms and applications of plasmon-induced charge separation at TiO_2 films loaded with gold nanoparticles, J. Am. Chem. Soc., 127 (2005) 7632-7637.

[21] A. Primo, A. Corma, H. García, Titania supported gold nanoparticles as photocatalyst, Phys. Chem. Chem. Phys., 13 (2010) 886-910.

[22] Z.F. Bian, J. Zhu, F.L. Cao, Y.F. Lu, H.X. Li, In situ encapsulation of Au nanoparticles in mesoporous core-shell TiO2 microspheres with enhanced activity and durability, Chem. Commun., (2009) 3789-3791.

[23] R.J. Dillon, J.B. Joo, F. Zaera, Y.D. Yin, C.J. Bardeen, Correlating the excited state relaxation dynamics as measured by photoluminescence and transient absorption with the photocatalytic activity of Au@TiO_2 core-shell nanostructures, Phys. Chem. Chem. Phys., 15 (2013) 1488-1496.

[24] N. Zhang, S.Q. Liu, X.Z. Fu, Y.J. Xu, Synthesis of M@TiO_2 (M = Au, Pd, Pt) Core-Shell Nanoconnposites with Tunable Photoreactivity, J. Phys. Chem. C, 115 (2011) 9136-9145.

[25] X.F. Wu, H.Y. Song, J.M. Yoon, Y.T. Yu, Y.F. Chen, Synthesis of Core-Shell Au@TiO_2 Nanoparticles with Truncated Wedge-Shaped Morphology and Their Photocatalytic Properties, Langmuir, 25 (2009) 6438-6447.

[26] S.H. Liu, S.Q. Bai, Y.G. Zheng, K.W. Shah, M.Y. Han, Composite Metal-Oxide Nanocatalysts, ChemCatChem, 4 (2012) 1462-1484.

[27] H. Hata, S. Kubo, Y. Kobayashi, T.E. Mallouk, Intercalation of well-dispersed gold nanoparticles into layered oxide nanosheets through intercalation of a polyamine, J. Am. Chem. Soc., 129 (2007) 3064-3065.

[28] T. Sasaki, M. Watanabe, H. Hashizume, H. Yamada, H. Nakazawa, Macromolecule-like aspects for a colloidal suspension of an exfoliated titanate. Pairwise association of nanosheets and dynamic reassembling process initiated from it, J. Am. Chem. Soc., 118 (1996) 8329-8335.

[29] T. Sasaki, M. Watanabe, Osmotic swelling to exfoliation. Exceptionally high degrees of hydration of a layered titanate, J. Am. Chem. Soc., 120 (1998) 4682-4689.

[30] T. Sasaki, Y. Ebina, Y. Kitami, M. Watanabe, T. Oikawa, Two-dimensional diffraction of molecular nanosheet crystallites of titanium oxide, J. Phys. Chem. B, 105 (2001) 6116-6121.

[31] T. Sasaki, M. Watanabe, Semiconductor nanosheet crystallites of quasi-TiO_2 and their optical properties, J. Phys. Chem. B, 101 (1997) 10159-10161.

[32] C.C. Chang, H.L. Wu, C.H. Kuo, M.H. Huang, Hydrothermal synthesis of monodispersed octahedral gold nanocrystals with five different size ranges and their self-assembled structures, Chem. Mater., 20 (2008) 7570-7574.

[33] T. Butburee, Y, Bai, J. Pan, X, Zong, C.H. Sun, G. Liu, L. Z. Wang, Step-wise controlled growth of metal@TiO_2 core-shells with plasmonic hot spots and their photocatalytic properties. J. Mater. Chem. A., 2 (2014), 12776-12784.

[34] G. Liu, L. Wang, C. Sun, Z. Chen, X. Yan, L. Cheng, H.M. Cheng, G.Q.M. Lu, Nitrogen-doped titania nanosheets towards visible light response, Chem. Commun., (2009) 1383-1385.

[35] T.W. Kim, S.J. Hwang, Y. Park, W. Choi, J.H. Choy, Chemical bonding character and physicochemical properties of mesoporous zinc oxide-layered titanate nanocomposites, J. Phys. Chem. C, 111 (2007) 1658-1664.

[36] T.W. Kim, S.G. Hur, S.J. Hwang, J.H. Choy, Layered titanate-zinc oxide nanohybrids with mesoporosity, Chem. Commun., (2006) 220-222.

[37] T.W. Kim, S.J. Hwang, S.H. Jhung, J.S. Chang, H. Park, W. Choi, J.H. Choy, Bifunctional Heterogeneous Catalysts for Selective Epoxidation and Visible Light Driven Photolysis: Nickel Oxide-Containing Porous Nanocomposite, Adv. Mater., 20 (2008) 539-542.

[38] K. Fukuda, Y. Ebina, T. Shibata, T. Aizawa, I. Nakai, T. Sasaki, Unusual crystallization behaviors of anatase nanocrystallites from a molecularly thin titania nanosheet and its stacked forms: Increase in nucleation temperature and oriented growth, J. Am. Chem. Soc., 129 (2007) 202-209.

[39] K.S.W. Sing, D.H. Everett, R.A.W. Haul, L. Moscou, R.A. Pierotti, J. Rouquerol, T. Siemieniewska, Reporting Physisorption Data For Gas Solid Systems with Special Reference to the Determination of Surface Area and Porosity (Recommendations 1984), Pure Appl. Chem., 57 (1985) 603-619.

[40] T.W. Kim, H.W. Ha, M.J. Paek, S.H. Hyun, I.H. Baek, J.H. Choy, S.J. Hwang, Mesoporous iron oxide-layered titanate nanohybrids: Soft-chemical synthesis, characterization, and photocatalyst application, J. Phys. Chem. C, 112 (2008) 14853-14862.

[41] W.B. Hou, W.H. Hung, P. Pavaskar, A. Goeppert, M. Aykol, S.B. Cronin, Photocatalytic Conversion of CO_2 to Hydrocarbon Fuels via Plasmon-Enhanced Absorption and Metallic Interband Transitions, ACS Catal., 1 (2011) 929-936.

[42] Y. Tian, T. Tatsuma, Mechanisms and applications of plasmon-induced charge separation at TiO_2 films loaded with gold nanoparticles, J. Am. Chem. Soc., 127 (2005) 7632-7637.

[43] O. Rosseler, M.V. Shankar, M.K.L. Du, L. Schmidlin, N. Keller, V. Keller, Solar light photocatalytic hydrogen production from water over Pt and Au/TiO_2(anatase/rutile) photocatalysts: Influence of noble metal and porogen promotion, J. Catal., 269 (2010) 179-190.

[44] S.W. Chen, R.W. Murray, Electrochemical quantized capacitance charging of surface ensembles of gold nanoparticles, J. Phys. Chem. B, 103 (1999) 9996-10000.

[45] V. Subramanian, E.E. Wolf, P.V. Kamat, Catalysis with TiO_2/gold nanocomposites. Effect of metal particle size on the Fermi level equilibration, J. Am. Chem. Soc., 126 (2004) 4943-4950.

[46] D. Andreescu, T.K. Sau, D.V. Goia, Stabilizer-free nanosized gold sols, J. Colloid Interface Sci., 298 (2006) 742-751.

[47] A.M. Schwartzberg, T.Y. Olson, C.E. Talley, J.Z. Zhang, Synthesis, characterization, and tunable optical properties of hollow gold nanospheres, J. Phys. Chem. B, 110 (2006) 19935-19944.

[48] C. Noguez, Surface plasmons on metal nanoparticles: the influence of shape and physical environment, J. Phys. Chem. C, 111 (2007) 3806-3819.

[49] Z. Liu, W. Hou, P. Pavaskar, M. Aykol, S.B. Cronin, Plasmon resonant enhancement of photocatalytic water splitting under visible illumination, Nano Lett., 11 (2011) 1111-1116.

[50] W.B. Hou, Z.W. Liu, P. Pavaskar, W.H. Hung, S.B. Cronin, Plasmonic enhancement of photocatalytic decomposition of methyl orange under visible light, J. Catal., 277 (2011) 149-153.

[51] J.J. Chen, J.C.S. Wu, P.C. Wu, D.P. Tsai, Plasmonic Photocatalyst for H_2 Evolution in Photocatalytic Water Splitting, J. Phys. Chem. C, 115 (2011) 210-216.

[52] P. Christopher, H. Xin, A. Marimuthu, S. Linic, Singular characteristics and unique chemical bond activation mechanisms of photocatalytic reactions on plasmonic nanostructures, Nat. Mater., 11 (2012) 1044-1050.

[53] C. Burda, X.B. Chen, R. Narayanan, M.A. El-Sayed, Chemistry and properties of nanocrystals of different shapes, Chem. Rev., 105 (2005) 1025-1102.

[54] D.D. Evanoff, G. Chumanov, Synthesis and optical properties of silver nanoparticles and arrays, ChemPhysChem, 6 (2005) 1221-1231.

[55] Y.-F. Wang, K.-N. Li, Y.-F. Xu, C.-Y. Su, D.-B. Kuang, Hierarchical Zn_2SnO_4 nanosheets consisting of nanoparticles for efficient dye-sensitized solar cells, Nano Energy, 2 (2013) 1287-1293.

Supporting information

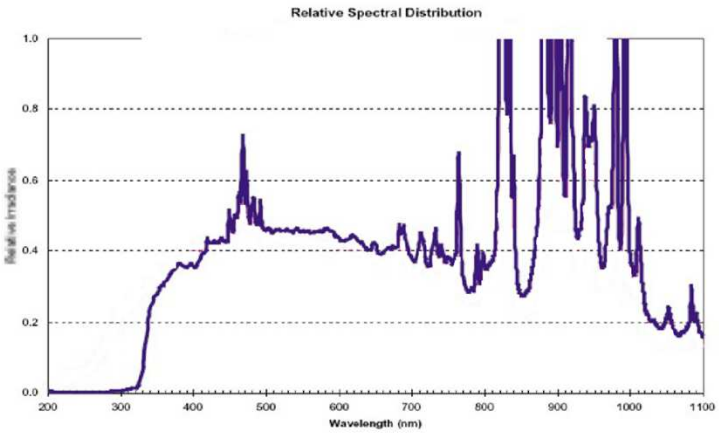

Figure S1. Light spectrum of the Xe lamp.